ORIGINAL ARTICLE

Characterizing the Flow and Interaction of Microbubbles in a 2D Capillary Network for Targeted Drug Delivery: A Simulation Study

Sadegh Shurche * , **Akram Shahidani, Roghaye Bodaghi Hossein Abadi**

Department of Medical Physics, School of Medical Sciences, Tarbiat Modares University, Tehran, Iran

*Corresponding Author: Sadegh Shurche
Email: sadegh.shurche@modares.ac.ir

Received: 04 April 2023 / Accepted: 14 October 2023

Abstract

Purpose: Microbubble ultrasound contrast agents inside the bloodstream enhance the ultrasound signals of the vascular bed. In addition, microbubbles can be used for treatment. The present study assesses how air bubbles flow in a microchannel 2D capillary network. The evaluated network mimics part of a capillary system by comprising multiple bifurcations.

Materials and Methods: We designed the capillary network based on the tree pattern employed in quantitative studies per Murray's minimum work rule and the cardiovascular network to simulate the hemodynamics of the vessels. The maximum width of the main channels in the capillary network is 1085 µm. The capillary network designed by AutoCAD software was transferred to Comsol software. We also ran fluid-structure interaction simulations in a microchannel capillary network, assuming that capillary walls were incompressible and isotropic, physiological boundary conditions were met, and non-Newtonian blood behavior occurred. After these simulations, we investigated Microbubbles' (MBs') capacity for targeted drug delivery through the capillary network. Specifically, we distributed four particles with 1 to 5 µm diameters and assessed the resultant performance.

Results: The greatest capillary network wall displacement is 0.225 µm. Meanwhile, the maximum velocity was 5.59 mm/s, and the minimum and maximum pressure values were 303.13 Pa and 0.42 Pa. Finally, the MB-MB interaction force exceeded the Brownian and gravitational forces. Therefore, it can be concluded that the MB-MB interaction force is crucial for MB-based targeted drug delivery. The kinetic energy of microbubbles increases while passing through the capillary bed. By increasing the amount of kinetic energy of microbubbles, the probability of adhesion to the capillary wall decreases. As the diameter of microbubbles increases, their energy increases.

Conclusion: The kinetic energy of microbubbles in the same conditions is the highest value related to Sonovue and then related to Optison, Micromarker, and Definity, respectively. The highest percentage of passing through the capillary network belongs to the Sonovue with a diameter of 2.5 µm and the lowest percentage of passing through the capillary network belongs to the Definity with a diameter of 1.1 µm.

Keywords: Blood Flow; Microbubble; Microcirculation; Drug Delivery.

DOI: https://doi.org/10.18502/fbt.v12i1.17733

1. Introduction

The presence of gas bubbles in the bloodstream can pose both hazards and potential therapeutic benefits. These bubbles can form when individuals experience sudden pressure changes, such as in scuba diving [1], space operations [2], or high-altitude flight [3]. They can also occur due to pathological conditions like heart valve damage [4, 5]. Additionally, air can be unintentionally or intentionally injected into patients during medical procedures like surgeries [6, 7], hemodialysis [8], or embolotherapy [1]. If left uncontrolled, these bubbles can restrict the supply of oxygen, leading to tissue damage, disability, or even death [9]. However, gas bubbles also have beneficial uses in medical diagnosis and treatment. They can serve as probes to improve image contrast in ultrasound examinations at specific frequencies [10]. Moreover, they can be utilized to restrict blood supply to tumors, inducing tumor necrosis, by blocking the vessels in tumorous tissues [11].

Much attention has been given to micro- and nanoparticles for targeted drug delivery [12, 13]. It has been proposed that the adhesion of particles and their ability to migrate to a target site is enhanced when they have the optimal diameter and shape [14, 15]. Research has also revealed a number of critical factors that affect the optimization of particles in terms of their shape and size: namely, their vessel geometry, blood velocity, and blood pressure. Optimizing these factors can also impact how effectively particles migrate and adhere to targeted surfaces [16].

There are various ways to make drug delivery more effective, including the use of Microbubbles (MBs) and ultrasound [17, 18]. Depending on the type of vessel being dealt with, different MBs can be employed for targeted drug delivery. Research has indicated multiple factors that influence the effectiveness of targeted drug delivery; these include the material comprising the MB's shell, the core gas used, the MB production process, the ultrasound method used, and the materials and targeting ligands employed [19, 20]. The MBs used in clinical and experimental settings consist of two parts: a core and a stabilizing membrane. The core contains perfluorocarbons, and the stabilizing membrane comprises various materials, including polymers, phospholipids, and proteins. The diameter of an MB depends on the species; however, in pharmacy settings, the typical diameter of particles is 1–5 μm, although diameters as large as 10 μm have been reported [21, 22].

Initially, researchers began paying attention to designing drug-loaded MBs to target cardiovascular tissues. Later, they began investigating liposome, which is a potentially powerful tool for targeted drug delivery [23]. Researchers have also examined the ability of drug carriers to target endothelial cells [24, 25].

The present work mimics a capillary system region by employing a microchannel capillary network. We also ran Fluid-Structure Interaction (FSI) simulations of a microchannel capillary network. Within this network, we considered physiological boundary conditions, incompressible and isotropic arterial wall behavior, and non-Newtonian blood behavior. Then, MBs were employed to target drug delivery in a capillary network. Definity, Micromarker, Optison, and Sonovue MBs were among the commercially approved MBs used in our simulation. We examined the size of MBs as a function of several relevant factors, including surface adhesion. Finally, we examined how the forces exerted on MBs affect the delivery of particles to the targeted surface.

2. Materials and Methods

This section describes the methods employed to design the capillary network geometry, as well as the methods used to determine the mechanical properties of the blood and the capillary wall. Next, we conducted the mesh study and evaluated the extent to which the solution depended on time. We also expressed the boundary condition of the simulation and the formulation of the FSI, and we presented each MB's mechanical properties. Furthermore, we explained the particle tracking process for fluid flow for the motion of MBs within the capillary network. Finally, we formulated the force applied by blood flow to MBs and the MB-MB forces.

2.1. Capillary Network Design

This section describes the capillary network, which we have employed in previous studies [26]. We designed the capillary network based on the tree pattern employed in quantitative studies per Murray's

minimum work rule and the cardiovascular network [27] to simulate the hemodynamics of the vessels.

We applied various calculations to the capillary network based on previous theories. Thereafter, we utilized AutoCAD software (M.49.0.0 AutoCAD 2016, Autodesk, Inc., San Rafael, CA, USA) to design the capillary network based on the parameters derived from the calculations (see Figure 1).

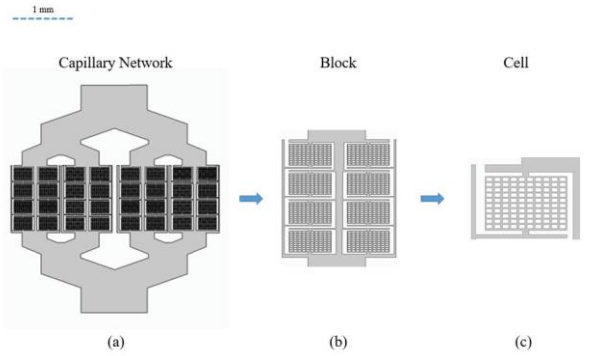

Figure 1. (a) The design of a capillary network and an enlarged view of the blocks and cells' layout. (b) The capillary network consists of four blocks, and its width is 15.506 mm. (c) Each of the four blocks has eight cells, each with 100 features. 25-µm wide channels through which the microbubbles pass separate these features

2.2. Capillary Wall and Blood Properties

The isotropic Raghavan et al. strain energy density model has been employed to describe the mechanical properties of the capillary wall. The strain energy density function is as follows [28] (Equation 1):

$$W_{iso} = C_{10}(I_1 - 3) + C_{20}(I_1 - 3)^2 + \frac{(J-1)^2}{d} \qquad (1)$$

In the equation above, W_{iso} represents the material's strain energy density. Meanwhile, the material constants are represented by C_{10} and C_{20}. The first deviatoric strain invariant is indicated by I_1, while J.

Denotes the ratio of deformed elastic voluminous materials to undeformed volume materials. Finally, d represents the incompressibility of the material. See Table 1 for details regarding the mechanical properties of the capillary wall.

The properties of blood can be described using the Carreau-Yasuda model [30]. See Table 2 for the values inserted for different parameters in Carreau-Yasuda model.

2.3. FSI and Boundary Conditions

We utilized the arbitrary Lagrangian-Eulerian (ALE) method to combine solid mechanics considering a Lagrangian description and a material frame with fluid formulated using Eulerian description, as well as a spatial frame. Navier-Stokes equations cannot be employed to measure the motion of fluid because fluid has non-Newtonian properties. However, incompressible non-Newtonian fluids can be modeled using generalized Newtonian fluids [31-33]. The equations for which consider apparent dynamic viscosity, the continuity equations are as follows [32] (Equation 2a, 2b):

$$\rho \frac{\partial u}{\partial t} + \rho u.\nabla u = -\nabla p + \nabla \tau \qquad (2a)$$

$$\nabla . u = 0 \qquad (2b)$$

Table 1. Material properties for capillary wall [29]

Hyperelastic model	C20[MPa]	C20[MPa]	D [Dimensionless]	ρ[kg/m^3]
Capillary	0.147	1.881	1.149	1120

Table 2. Carreau–Yasuda model values for the related parameters [30]

Hematocrit percentage	η_0 [Pa.s]	λ[s]	α [Dimensionless]	η_∞ [Pa.s]
25%	0.018	12.448	0.330	0.00257
45%	0.161	39.418	0.479	0.00345
65%	0.852	103.088	0.389	0.00802

Where ρ, u, and p are the density, the velocity vector, and the pressure of the fluid, respectively. Moreover, the stress tensor components τ_{ij} are proportional to the strain rate tensor components S_{ij} as follows [31] (Equation 3a, 3b):

$$\tau_{ij} = 2\eta_{app}S_{ij} - p\delta_{ij} \quad (3a)$$

$$S_{ij} = \frac{1}{2}\left(\frac{\partial u_i}{\partial x_j} + \frac{\partial u_j}{\partial x_i}\right) - \frac{1}{3}\frac{\partial u_k}{\partial x_k}\delta_{ij} \quad (3b)$$

Here, δ_{ij} is the Kronecker delta function defined as follows (Equation 4) [34]:

$$\delta_{ij} = \begin{cases} 1 & \text{if } i=j \\ 0 & \text{if } i \neq j \end{cases} \quad (4)$$

The blood in a capillary interacts with the capillary wall. As a result, the capillary wall experiences a force. The following equation calculates the total force, f, exerted on the solid boundary [35] (Equation 5):

$$f = n.[-pI + \eta_{app}\left[(\nabla u + (\nabla u)^T) - \frac{2}{3}(\nabla . u)I\right)] \quad (5)$$

Where n is the boundary's outward normal vector, I denotes the identity matrix, and the fluid's apparent dynamic viscosity is symbolized by η_{app}.

Regarding the relation between vessel diameter and blood velocity, values were taken from the literature and inserted into the plot generated by simulations. Centerline velocities (v_c) were determined in the arteries by Kobari *et al.* [36], who used Equation 6 to determine velocity as a function of diameter (in μm):

$$V_c = (0.034d + 0.309) \quad (6)$$

2.4. MBs and Their Properties

We considered four MB types (Definity MBs, Micromarker MBs, Optison MBs, and Sonovue MBs) when performing the targeted delivery process. Typical Definity MBs have a lipid cell comprising phospholipids (DPPC, DPPA, and MPEG5000DPPPE) with a gas core. These MBs also contain nitrogen and perfluorobutane gas (C_4F_{10}) [37, 38]. Optison MBs consist of human serum albumin cells with a (C_3F_8) gas core. Sonovue MBs consist of a lipid cell consisting of zwitterionic phosphatidylcholine, as well as an anionic phospholipid with an SF_6 gas core [38-41]. We set the density of MBs to 1000 Kg/m^3 for this study [42]. See Table 3 for the MBs' specific mechanical properties.

2.5. Particle Tracking for Fluid Flow

At the inlet section of the capillary network in the simulation, 30, 130, and 300 MBs with the properties described above (see Section 2.5) were released in intervals of one second. The injection times were set to zero, one, two, and three seconds.

We utilized a mixed scattering diffusion method to obtain valid MB characteristics in blood flow. Furthermore, for the arterial wall-MBs interactions, we simulated the impact of unsmooth endothelial surfaces on the motion of MBs using the specular reflection method. The probability of an MB being reflected specularly was γ = 0.5. MBs are reflected from the surface of the tangent plane during specular reflection.

2.6. Forces Exerting on the Released Particles

The two forces were exerted on the MBs: one was produced by the external field, and the other was the interaction force between MBs (Figure 2). The finite element method was used to determine the strength of the first kind of force. During this process, the new locations of MBs were queried at each time step,

Table 3. Material properties for MBs

Agent formulation	Shell	Gas	Diameter (μm)	Surface tension (N/m)	Dynamic viscosity (Pa.s)	Elasticity (N/m)	Reference
Definity	Lipid	C_3F_8	1.1–3.3	0.051	0.00415	0.855	[37, 38]
Micromarker	Phospholipid	C_4F_{10}	2.0–5.0	0.051	0.00952	5.150	[37, 38]
Optison	Albumin	C_3F_8	3.0–4.5	0.072	0.001	0.230	[38, 39]
Sonovue	Phospholipid	SF_6	1.5–2.5	0.073	0.001	0.55	[40, 41]

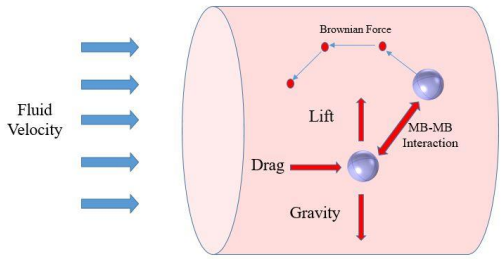

Figure 2. Forces, which act on an MB in a fluid

according to the external forces. The second kind of force was then added to the total force. Subsequently, the MBs' positions were updated. We repeated these for the duration of the simulation.

Newton's second law for moving MBs with a mass of m_p, can be expressed as Equation 7:

$$\frac{d}{dt}(m_p v) = F_d + F_L + F_B + F_G \quad (7)$$

Where m_p represents each particle's mass and v denotes each particle's velocity vector. F_D, F_L, F_B, and F_G represent meanwhile, the drag force, lift force, Brownian force, and gravitational forces acting on MBs, respectively.

2.7. MB Adhesive Dynamic Model

In the current study, it was hypothesized that the MB surface is covered by a P-Selectable Aptamer (PSA). These aptamers are of a higher adhesion tendency than any antibodies in previous studies [43]. The ligand-receptor binding equation was first introduced by Decuzzi and Ferrari to calculate the sticking probability of particles [44]. Their model's force, torque, and T were applied to the sphere particles under fluid Flow; wall shear strain distorted their shape and size (Equations 8, 9):

$$F = 3\pi d_p l \eta_{app} S F^s \quad (8)$$

$$T = \frac{1}{2}\pi d_p^3 \eta_{app} S T^s \quad (9)$$

Where l is the separation distance of the particles from the substrate and the F^s and T^s are two parameters depending on the particle aspect ratio ($\gamma = a/b$). In the study of spherical particles $\gamma = 1$ the classical results in research by Goldman and his colleagues [45] were selected; $F^s = 1.668$ s and $T^s = 0.944$.

In the limit of a small surface density of receptors m_r or ligands m_l the probability of adhesion, P_a for spherical particles has the following form (Equations 10, 11):

$$P_a = \pi r_0^2 m_r m_l K_a^0 \times exp\left[-\frac{\beta d_p \eta_{app} S}{k_B T r_0^2 m_r}\left[3\left(\frac{d_p}{2} + \delta_{eq}\right)F^s + \frac{d_p^2}{r_0}T^s\right]\right] \quad (10)$$

$$r_0^2 = d_p^2\left[\frac{1}{4} - \left[\frac{1}{2} - \frac{(h_0 - \delta_{eq})}{d_p}\right]^2\right] \quad (11)$$

Where K_a is the association constant at zero loads of the ligand–receptor bound, β is the reactive compliance which is usually in the order of Angstrom, δ_{eq} is the equilibrium separation distance between the spheroidal particle and the vascular substrate, k_BT is the Boltzmann thermal energy, h_0 is the maximum distance of the particle from the vascular wall at which a specific bond can take place, and r_0 is the radius of the circular section of the spheroid situated at a separation distance h_0 from the substrate.

The values of their parameters are presented in Table 4.

Table 4. The corresponding values of parameters that apply to the PSA adhesion dynamics model: P-selecting

Parameter	Value
Intrinsic forward kinetic rate: K_f (S^{-1})	2.33×10^5
Intrinsic reverse kinetic rate: K_r (S^{-1})	3.4×10^{-5}
Equilibrium bond length: δ_{eq} (nm)	50
Reactive compliance: β (Å)	0.21
Boltzmann's constant: K_B (m^2 kg/ s^2K)	1.3806×10^{-23}
Surface density of receptors: m_r(m^{-2})	2.7×10^{15}
Temperature: T(K)	310.15
Shear stress at the wall: $\eta_{app}S$ (Pa)	Obtained from the FSI simulation

3. Results

We employed COMSOL Multiphysics 5.6 to solve various partial differential equations. We also used a

tolerance termination procedure and a PDF time-stepping technique to simulate the FSI (e.g. the MUMPs algorithm). Furthermore, we utilized a solver involving backward Euler consistent initialization, as well as the generalized-alpha time-stepping method, to simulate the process of MB transport [1, 46, 47].

3.1. FSI Results

The maximum displacement of a capillary wall must be restricted to a specific range to prevent the capillary network from rupturing. As indicated in Figure 3, the maximum displacement is 0.225 µm.

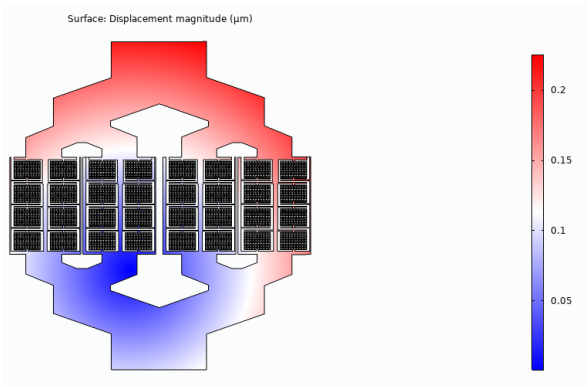

a

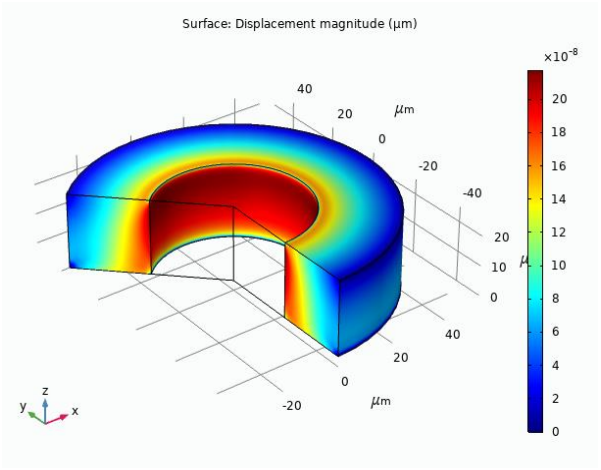

b

Figure 3. The amount of displacement (µm) of the walls during the passage of blood through the (a) capillary network and (b) in a capillary *(Generated by COMSOL Multiphysics 5.6, https://www.comsol.com*)

The velocity in the capillary network is shown in Figure 4. Since the diameter of the arteriole inlet is 1085 µm according to the design and calculations, according to Equation 6, the inlet velocity was

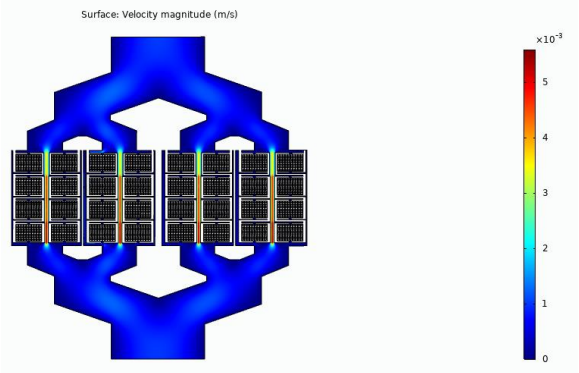

a

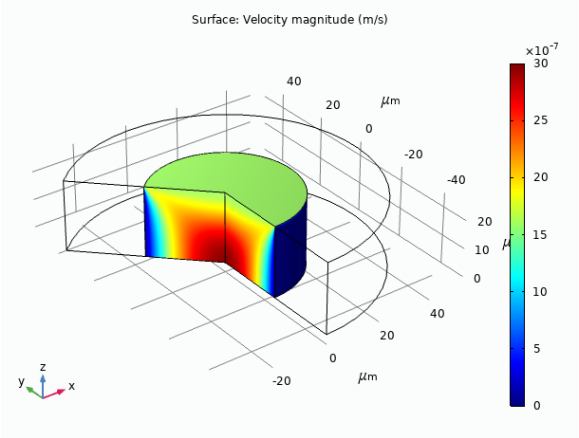

b

Figure 4. Flow surface colored by velocity magnitude (m/s) for (a) the entire capillary network and (b) a capillary (Generated by COMSOL Multiphysics 5.6, https://www.comsol.com)

considered 37.199 µm per second. The maximum velocity in the capillary network was 5.59 mm/s.

The pressure in the capillary network is shown in Figure 5. The maximum pressure in the capillary network was 303.13 Pa and the minimum pressure was 0.42 Pa.

The distribution of four types of microbubbles in the capillary network was obtained. Figure 6 shows the distribution of microbubbles with a diameter of 1.1 µm in numbers of 30, 130, and 300.

The distribution and movement of microbubbles, for example, are shown in Figure 7, which is for microbubbles with a diameter of 1.1 µm and a number of 300.

The energy change of microbubbles while passing through the capillary network is shown in Figure 8.

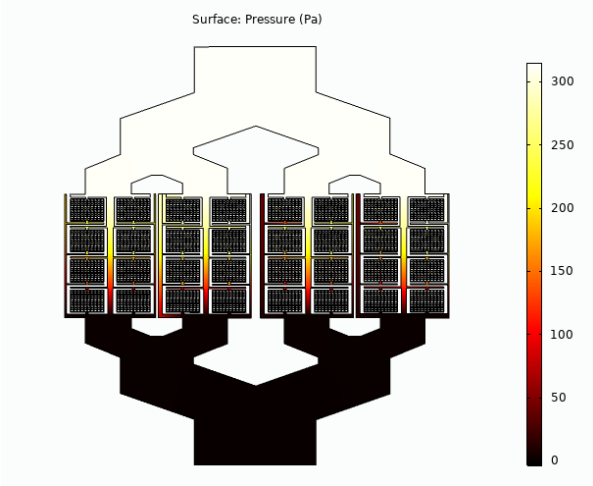

a

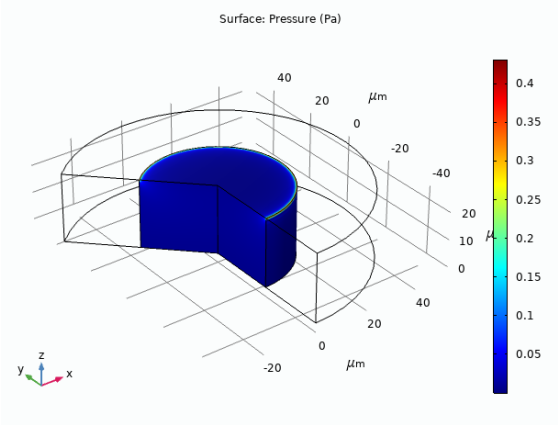

b

Figure 5. Flow surface colored by pressure magnitude (m/s) for (a) the entire capillary network and (b) a capillary (Generated by COMSOL Multiphysics 5.6, https://www.comsol.com)

3.2. Brownian, Gravitational, and MB-MB Interaction Force

Recent research indicates that Brownian forces interfere with solid particles on the μm scale and that the impact of such forces is Significant on the nanometer scale [17]. Therefore, during the simulation, we considered the Brownian force by investigating its effect on SDM adhesion. We examined SDM adhesion both with and without considering Brownian forces (Figure 9). We considered a minimum diameter of 1.1 μm to evaluate the effect of the Brownian forces. As Figure 9 indicates, Brownian forces' effect on SDM adhesion did not reach 10%, meaning this effect was much lower than those reported in recent studies on solid nanoscale particles [35].

We applied a maximum diameter of five μm to demonstrate the effect of gravitational force. As shown in Figure 9, gravitational force had a weak negative effect (~7.3%) on MBs and a positive effect on surface adhesion [35]. The main reason for gravitational force's negative effect on MBs could be the density of the particles containing the drug. Unlike solid particles, MBs are less dense than blood, meaning that gravitational force hinders SDM adhesion.

The smaller the diameter of MBs, the greater the MB-MB interaction force. Because of this, we used one μm (i.e. the smallest MB diameter examined) when evaluating MB-MB interaction forces' impact on SDM adhesion. The results show that, on the lumen AAA, MB-MB interaction force had an impact of

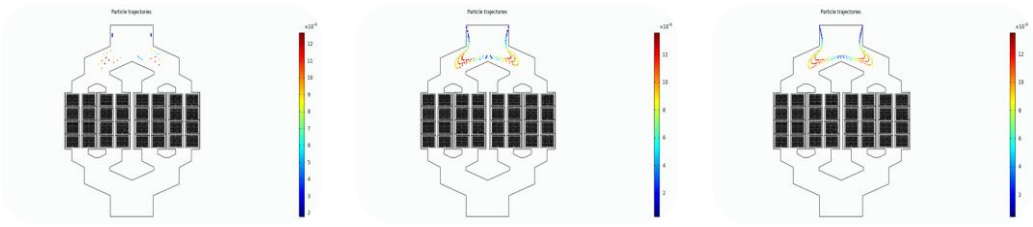

(a) (b) (c)

Figure 6. (a). The distribution of microbubbles with a size of 1.1 μm in the capillary network in the number of 30 pieces. (b). The distribution of microbubbles with a size of 1.1 μm in the capillary network in the number of 130 pieces. (c). The distribution of microbubbles with a size of 1.1 μm in the capillary network in the number of 300 pieces

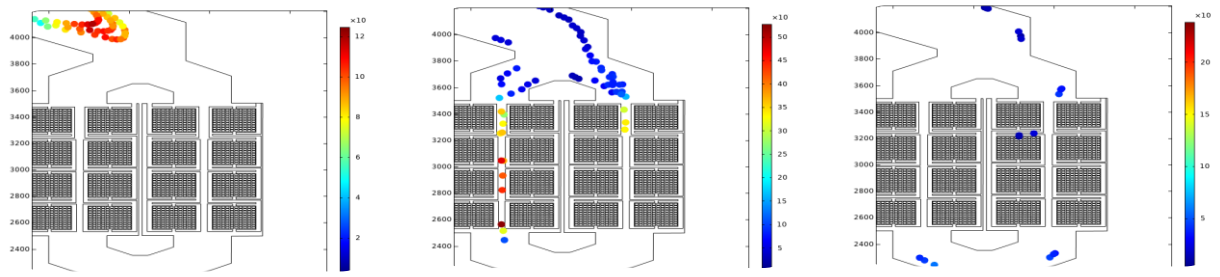

1 s 2 s 3 s

Figure 7. The distribution and movement of microbubbles with a diameter of 1.1 µm and a number of 300 in the capillary network are shown

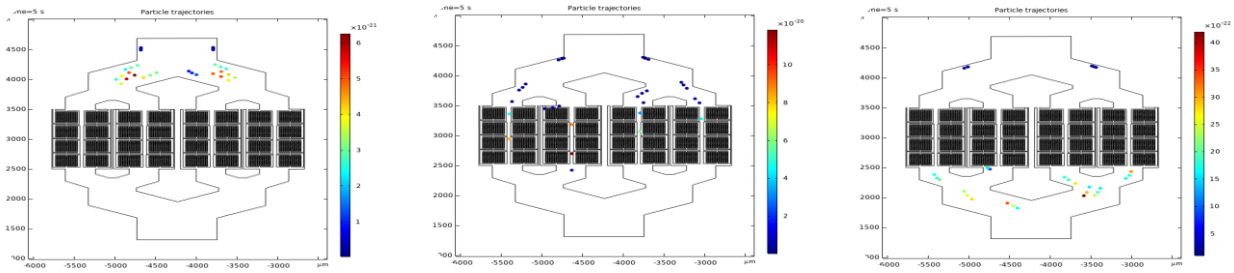

1 s 2 s 3 s

Figure 8. Energy change of microbubbles (Sonovue) with a diameter of 2.5 µm while passing through the capillary network

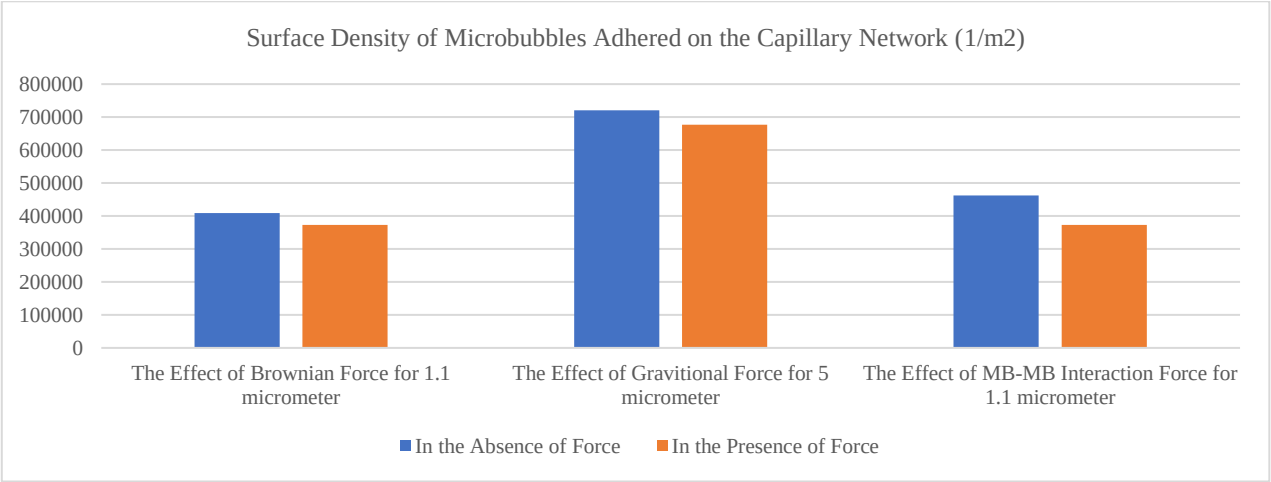

Figure 9. Variation of the SDM adhesion on the capillary network to check the effect of the Brownian, gravitational, and MB-MB interaction forces

~19.2 percentage on SDM adhesion (Figure 9). This impact exceeds both the Brownian and gravitational forces. As such, this finding indicates that the MB-MB interaction force is crucial to MB-based targeted drug delivery.

3.3. The Percentage of Microbubbles Passing Through the Capillary Network

The amount of microbubbles passing through the capillary network for the number of different inlets

Table 5. Microbubble passage through the capillary network based on the number, type, and size of microbubbles

Microbubble type	Number of entries	Size (µm)	Number of entrapped microbubbles	Microbubbles pass percentage
Definity	30	1.1	14	54
		3.3	11	64
	130	1.1	28	79
		3.3	25	81
	300	1.1	46	85
		3.3	41	87
Micromarker	30	2	11	64
		5	9	70
	130	2	24	82
		5	20	85
	300	2	43	86
		5	39	87
Optison	30	3	8	74
		4.5	6	80
	130	3	22	84
		4.5	19	86
	300	3	41	87
		4.5	36	88
Sonovue	30	1.5	6	80
		2.5	4	87
	130	1.5	20	85
		2.5	18	87
	300	1.5	39	87
		2.5	35	89

and the type of microbubbles and the size of the microbubbles are shown in Table 5.

4. Discussion

We investigated the distribution of microbubbles in a simulated capillary network and recorded a maximum capillary network wall displacement of 0.225 µm (Figure 3), as well as a maximum velocity of 5.59 mm/s (Figure 4), which is supported by the findings of Ivanov *et al.* [48]. Furthermore, the results indicate a maximum capillary network pressure of 303.13 Pa, while the minimum pressure value recorded was 0.42 Pa (Figure 5). These findings align with a previous study conducted by Shore *et al.* [49. The current assessment of the forces applied to the MBs during intra-capillary drug delivery enhances the current knowledge of how such forces affect SDM adhesion. The simulation results show a linear increase in the drag force applied to various MB types as the particle diameter increased. Increases in particle diameter also caused a quadratic increase in the lift force exerted on MBs. However, lift force did not significantly affect adhesion as indicated by the results comparing MB adhesion in the capillary network when these forces were and were not considered (Figure 9). The results revealed a significant effect of Brownian forces and MB-MB interactions on the adhesion of drug-carrying MBs to the capillary network wall.

However, the extant literature indicates that ultrasound wave forces cause MBs to burst by oscillating them to their critical point (i.e. the resonance point); at this point, linear displacement has a negligible effect [50]. Future studies should investigate whether acoustic waves affect the adhesion of SDM to the intended surface. The present study used the PSA type of particle adhesive dynamics model. However, recent research provides various particle adhesion models considering the receptor-ligand bond. Such models can be used to

evaluate SDM adhesion in more depth [35]. Furthermore, SDM adhesion to the intended surface, as well as the number of MBs exiting in dichotomy, can be used to optimize the number of MBs entering the capillary network. Recent research on electromagnetic MBs has shown that electromagnetic forces can be harnessed to deliver drugs to the target [51]. Future research should also study whether MB adhesion can be enhanced via the application of an electromagnetic field.

According to Figure 8, the energy of microbubbles changes while passing through the capillary network so that the amount of energy of microbubbles increases inside the capillary bed.

According to Figure 6, the distribution of microbubbles in the first branch of the daughter is the same in both directions, which is the same as the research results of Valassis *et al.* [52].

According to Figure 9, the amount of surface tension increases, which is caused by many branches of capillaries, while in a single capillary without branches, the amount of surface tension is lower, which is the same as the results of Valassis *et al.* [52].

The reverse microbubble was not observed in the flow path in the capillary network, which was similar to the results of Calderon *et al.* [53].

According to Figure 5, the flow pressure in smaller capillaries is lower, which is due to the greater resistance of these capillaries to the flow, which is in accordance with the results of Chao *et al.*'s [54] research, and this causes the microbubbles in them to flow less.

5. Conclusion

Simulations are useful tools for examining biological phenomena [16, 35, 55]. As such, we examined MB-based targeted drug delivery in a simulated capillary network. The kinetic energy of microbubbles in the same conditions is the highest value related to Sonovue and then related to Optison, Micromarker, and Definity respectively. The highest percentage of passing through the capillary network belongs to the Sonovue with a diameter of 2.5 µm and the lowest percentage of passing through the capillary network belongs to the Definity with a diameter of 1.1 µm.

References

1- Jintai Chung and GM1223971 Hulbert, "A time integration algorithm for structural dynamics with improved numerical dissipation: the generalized-α method." (1993).

2- Lars L Karlsson, S Lesley Blogg, Peter Lindholm, Mikael Gennser, Tryggve Hemmingsson, and Dag Linnarsson, "Venous gas emboli and exhaled nitric oxide with simulated and actual extravehicular activity." *Respiratory Physiology & Neurobiology*, Vol. 169pp. S59-S62, (2009).

3- Philip P Foster and Bruce D Butler, "Decompression to altitude: assumptions, experimental evidence, and future directions." *Journal of Applied Physiology*, Vol. 106 (No. 2), pp. 678-90, (2009).

4- Ghislaine Deklunder, Martine Roussel, Jean-Louis Lecroart, Alain Prat, and Corinne Gautier, "Microemboli in cerebral circulation and alteration of cognitive abilities in patients with mechanical prosthetic heart valves." *Stroke*, Vol. 29 (No. 9), pp. 1821-26, (1998).

5- Simcha Milo, Edmond Rambod, Chaim Gutfinger, and Morteza Gharib, "Mitral mechanical heart valves: in vitro studies of their closure, vortex and microbubble formation with possible medical implications." *European Journal of Cardio-Thoracic Surgery*, Vol. 24 (No. 3), pp. 364-70, (2003).

6- Michael A Borger, Charles M Peniston, Richard D Weisel, Marie Vasiliou, Robin EA Green, and Christopher M Feindel, "Neuropsychologic impairment after coronary bypass surgery: effect of gaseous microemboli during perfusionist interventions." *The Journal of Thoracic and Cardiovascular Surgery*, Vol. 121 (No. 4), pp. 743-49, (2001).

7- Yasir Abu-Omar, Lognathen Balacumaraswami, David W Pigott, Paul M Matthews, and David P Taggart, "Solid and gaseous cerebral microembolization during off-pump, on-pump, and open cardiac surgery procedures." *The Journal of Thoracic and Cardiovascular Surgery*, Vol. 127 (No. 6), pp. 1759-65, (2004).

8- Margaret D Bischel, Brian G Scoles, and John G Mohler, "Evidence for pulmonary microembolization during hemodialysis." *Chest*, Vol. 67 (No. 3), pp. 335-37, (1975).

9- Claus M Muth and Erik S Shank, "Gas embolism." *New England Journal of Medicine*, Vol. 342 (No. 7), pp. 476-82, (2000).

10- Wei-Lung Chou, Pee-Yew Lee, Cing-Long Yang, Wen-Ying Huang, and Yung-Sheng Lin, "Recent advances in applications of droplet microfluidics." *Micromachines*, Vol. 6 (No. 9), pp. 1249-71, (2015).

11- Brijesh Eshpuniyani, J Brian Fowlkes, and Joseph L Bull, "A boundary element model of microbubble sticking and sliding in the microcirculation." *International Journal*

of Heat and Mass Transfer, Vol. 51 (No. 23-24), pp. 5700-11, (2008).

12- Kathrin Müller, Dmitry A Fedosov, and Gerhard Gompper, "Understanding particle margination in blood flow–a step toward optimized drug delivery systems." *Medical Engineering & Physics*, Vol. 38 (No. 1), pp. 2-10, (2016).

13- Netanel Korin *et al.*, "Shear-activated nanotherapeutics for drug targeting to obstructed blood vessels." *Science*, Vol. 337 (No. 6095), pp. 738-42, (2012).

14- B Asgharian, Werner Hofmann, and Rudolf Bergmann, "Particle deposition in a multiple-path model of the human lung." *Aerosol Science & Technology*, Vol. 34 (No. 4), pp. 332-39, (2001).

15- Yaling Liu, Samar Shah, and Jifu Tan, "Computational modeling of nanoparticle targeted drug delivery." *Reviews in Nanoscience and Nanotechnology*, Vol. 1 (No. 1), pp. 66-83, (2012).

16- Mohamadamin Forouzandehmehr and Amir Shamloo, "Margination and adhesion of micro-and nanoparticles in the coronary circulation: a step towards optimised drug carrier design." *Biomechanics and Modeling in Mechanobiology*, Vol. 17 (No. 1), pp. 205-21, (2018).

17- Christian R Mayer, Nicolas A Geis, Hugo A Katus, and Raffi Bekeredjian, "Ultrasound targeted microbubble destruction for drug and gene delivery." *Expert opinion on drug delivery*, Vol. 5 (No. 10), pp. 1121-38, (2008).

18- Evan Unger, Thomas Porter, Jonathan Lindner, and Paul Grayburn, "Cardiovascular drug delivery with ultrasound and microbubbles." *Advanced Drug Delivery Reviews*, Vol. 72pp. 110-26, (2014).

19- Alexander L Klibanov, "Microbubble contrast agents: targeted ultrasound imaging and ultrasound-assisted drug-delivery applications." *Investigative Radiology*, Vol. 41 (No. 3), pp. 354-62, (2006).

20- Joseph L Bull, "The application of microbubbles for targeted drug delivery." *Expert opinion on drug delivery*, Vol. 4 (No. 5), pp. 475-93, (2007).

21- Jia-You Fang, Chi-Feng Hung, Mei-Hui Liao, and Chih-Chen Chien, "A study of the formulation design of acoustically active lipospheres as carriers for drug delivery." *European Journal of Pharmaceutics and Biopharmaceutics*, Vol. 67 (No. 1), pp. 67-75, (2007).

22- Donovan J May, John S Allen, and Katherine W Ferrara, "Dynamics and fragmentation of thick-shelled microbubbles." *IEEE Transactions on Ultrasonics, Ferroelectrics, and Frequency Control*, Vol. 49 (No. 10), pp. 1400-10, (2002).

23- Susan T Laing and David D McPherson, "Cardiovascular therapeutic uses of targeted ultrasound contrast agents." *Cardiovascular Research*, Vol. 83 (No. 4), pp. 626-35, (2009).

24- Michiel Postema, Ayache Bouakaz, J Folkert, Georg Schmitz, Nico De Jong, and Annemieke van Wamel, "Nitric oxide delivery by ultrasonic cracking: some limitations." *Ultrasonics*, Vol. 44pp. e109-e13, (2006).

25- Vladimir R Muzykantov, Ravi Radhakrishnan, and David M Eckmann, "Dynamic factors controlling targeting nanocarriers to vascular endothelium." *Current Drug Metabolism*, Vol. 13 (No. 1), pp. 70-81, (2012).

26- Sadegh Shurche and Mohammad Yousefi Sooteh, "Computational simulations of nanoparticle transport in a three-dimensional capillary network." *Nanomedicine Journal*, Vol. 6 (No. 4), pp. 291-300, (2019).

27- Cecil D Murray, "The physiological principle of minimum work: I. The vascular system and the cost of blood volume." *Proceedings of the National Academy of Sciences*, Vol. 12 (No. 3), pp. 207-14, (1926).

28- Fatma Gulden Simsek and Young W Kwon, "Investigation of material modeling in fluid–structure interaction analysis of an idealized three-layered abdominal aorta: aneurysm initiation and fully developed aneurysms." *Journal of Biological Physics*, Vol. 41 (No. 2), pp. 173-201, (2015).

29- ML Raghavan and David A Vorp, "Toward a biomechanical tool to evaluate rupture potential of abdominal aortic aneurysm: identification of a finite strain constitutive model and evaluation of its applicability." *Journal of Biomechanics*, Vol. 33 (No. 4), pp. 475-82, (2000).

30- Ohwon Kwon, Mahesh Krishnamoorthy, Young I Cho, John M Sankovic, and Rupak K Banerjee, "Effect of blood viscosity on oxygen transport in residual stenosed artery following angioplasty." *Journal of Biomechanical Engineering*, Vol. 130 (No. 1), (2008).

31- Fabio Gori and Andrea Boghi, "Two new differential equations of turbulent dissipation rate and apparent viscosity for non-newtonian fluids." *International communications in heat and mass transfer*, Vol. 38 (No. 6), pp. 696-703, (2011).

32- Andrey A Gavrilov and Valeriy Ya Rudyak, "Reynolds-averaged modeling of turbulent flows of power-law fluids." *Journal of Non-Newtonian Fluid Mechanics*, Vol. 227pp. 45-55, (2016).

33- AA Gavrilov and V Ya Rudyak, "Direct numerical simulation of the turbulent energy balance and the shear stresses in power-law fluid flows in pipes." *Fluid Dynamics*, Vol. 52 (No. 3), pp. 363-74, (2017).

34- What are the Radiation Risks from CT? (June 4 2022).and [Online]. Available: https://www.fda.gov/radiation-emittingproducts/medical-x-ray-imaging/what-are-radiation-risks-ct., ed.

35- Amir Shamloo, Ali Amani, Mohamadamin Forouzandehmehr, and Ibrahim Ghoytasi, "In silico study of patient-specific magnetic drug targeting for a coronary

LAD atherosclerotic plaque." *International Journal of Pharmaceutics,* Vol. 559pp. 113-29, (2019).

36- Masahiro Kobari, Fumio Gotoh, Yasuo Fukuuchi, Kortaro Tanaka, Norihiro Suzuki, and Daisuke Uematsu, "Blood flow velocity in the pial arteries of cats, with particular reference to the vessel diameter." *Journal of Cerebral Blood Flow and Metabolism,* Vol. 4 (No. 1), pp. 110-14, (1984).

37- Brandon L Helfield and David E Goertz, "Nonlinear resonance behavior and linear shell estimates for Definity™ and MicroMarker™ assessed with acoustic microbubble spectroscopy." *The Journal of the Acoustical Society of America,* Vol. 133 (No. 2), pp. 1158-68, (2013).

38- Shengping Qin, Charles F Caskey, and Katherine W Ferrara, "Ultrasound contrast microbubbles in imaging and therapy: physical principles and engineering." *Physics in Medicine and Biology,* Vol. 54 (No. 6), p. R27, (2009).

39- Jingfeng Guan and Thomas J Matula, "Using light scattering to measure the response of individual ultrasound contrast microbubbles subjected to pulsed ultrasound in vitro." *The Journal of the Acoustical Society of America,* Vol. 116 (No. 5), pp. 2832-42, (2004).

40- Philippe Marmottant *et al.*, "A model for large amplitude oscillations of coated bubbles accounting for buckling and rupture." *The Journal of the Acoustical Society of America,* Vol. 118 (No. 6), pp. 3499-505, (2005).

41- Mark A Borden and Kang-Ho Song, "Reverse engineering the ultrasound contrast agent." *Advances in colloid and interface science,* Vol. 262pp. 39-49, (2018).

42- Tom van Rooij, "Ultrasound contrast agents for imaging and therapy." (2017).

43- Amir Shamloo and Mohamadamin Forouzandehmehr, "Personalised deposition maps for micro-and nanoparticles targeting an atherosclerotic plaque: attributions to the receptor-mediated adsorption on the inflamed endothelial cells." *Biomechanics and Modeling in Mechanobiology,* Vol. 18pp. 813-28, (2019).

44- P Decuzzi and Mauro Ferrari, "The adhesive strength of non-spherical particles mediated by specific interactions." *Biomaterials,* Vol. 27 (No. 30), pp. 5307-14, (2006).

45- Arthur Joseph Goldman, Raymond G Cox, and Howard Brenner, "Slow viscous motion of a sphere parallel to a plane wall—I Motion through a quiescent fluid." *Chemical Engineering Science,* Vol. 22 (No. 4), pp. 637-51, (1967).

46- Uri M Ascher and Linda R Petzold, Computer methods for ordinary differential equations and differential-algebraic equations. *Siam*, (1998).

47- Charles Francis Curtiss and Joseph O Hirschfelder, "Integration of stiff equations." *Proceedings of the National Academy of Sciences,* Vol. 38 (No. 3), pp. 235-43, (1952).

48- KP Ivanov, MK Kalinina, and Yu I Levkovich, "Blood flow velocity in capillaries of brain and muscles and its physiological significance." *Microvascular Research,* Vol. 22 (No. 2), pp. 143-55, (1981).

49- Angela C Shore, "Capillaroscopy and the measurement of capillary pressure." *British Journal of Clinical Pharmacology,* Vol. 50 (No. 6), pp. 501-13, (2000).

50- Siew Wan Fong, Evert Klaseboer, and Boo Cheong Khoo, "Interaction of microbubbles with high intensity pulsed ultrasound." *The Journal of the Acoustical Society of America,* Vol. 123 (No. 3), pp. 1784-93, (2008).

51- Marie-Albane de Saint Victor, "Investigating magnetically targeted microbubbles for ultrasound-enhanced thrombolysis." *University of Oxford*, (2016).

52- Doug T Valassis, Robert E Dodde, Brijesh Esphuniyani, J Brian Fowlkes, and Joseph L Bull, "Microbubble transport through a bifurcating vessel network with pulsatile flow." *Biomedical Microdevices,* Vol. 14pp. 131-43, (2012).

53- Andres J Calderon, Brijesh Eshpuniyani, J Brian Fowlkes, and Joseph L Bull, "A boundary element model of the transport of a semi-infinite bubble through a microvessel bifurcation." *Physics of Fluids,* Vol. 22 (No. 6), (2010).

54- Cong Chao, Xiaoqiang Jin, and Xianfeng Fan, "Effect of network structure on the bubble dislodgment and pressure distribution in microfluidic networks with multiple bifurcations." *Chemical Engineering Science,* Vol. 209p. 115176, (2019).

55- Amir Shamloo, Farid Manuchehrfar, and Hashem Rafii-Tabar, "A viscoelastic model for axonal microtubule rupture." *Journal of Biomechanics,* Vol. 48 (No. 7), pp. 1241-47, (2015).